sustainability

MDPI

Article

Pulse Electrodeposition for Carbonate-Rich Deposits from Seawater

Alexander J. Robinson [1], Elisabeth A. Ryan [1], Qingpu Wang [2], David Greene [3] and Chinmayee V. Subban [1,2,*]

[1] Department of Materials Science and Engineering, University of Washington, Seattle, WA 98195, USA
[2] Energy and Environment Directorate, Pacific Northwest National Laboratory, Seattle, WA 98109, USA
[3] National Renewable Energy Laboratory, Golden, CO 80401, USA
* Correspondence: chinmayee.subban@pnnl.gov

Abstract: Seawater electrodeposition is gaining renewed interest in the context of sustainable development, both to build climate-resilient coastal infrastructure and for ocean-based decarbonization applications. Most of the applications benefit from $CaCO_3$-rich deposits, but constant-voltage electrodeposition results in a mixture of $CaCO_3$ and $Mg(OH)_2$, especially at higher voltages where precipitation rates are more desirable. The use of pulse voltages can help control interfacial pH that dictates the precipitation reactions. Here, we explore the use of pulse electrodeposition as a function of pulse frequency and duty cycle to control deposit composition. The most $CaCO_3$-rich deposits were obtained under 10 Hz frequency and 10% duty cycle conditions for the voltage window investigated (−0.8 V to −1.2 V vs. SCE). While pulsing the voltage increases the amount of $CaCO_3$ deposited, the energy required per gram of $CaCO_3$ is significantly higher (14.5×) when compared to the base case of applying a constant voltage of −0.8 V vs. SCE. Further optimization of pulse conditions, electrode materials, and system configuration could lead to finding parameters that result in exclusively carbonate deposits without compromising precipitation rates, which may prove to be more useful for corrosion protection, coastal infrastructure, and other applications in sustainable development.

Keywords: carbon mineralization; calcareous deposits; electrodeposition; voltage pulsing; seawater

Citation: Robinson, A.J.; Ryan, E.A.; Wang, Q.; Greene, D.; Subban, C.V. Pulse Electrodeposition for Carbonate-Rich Deposits from Seawater. *Sustainability* **2024**, *16*, 10776. https://doi.org/10.3390/su162310776

Academic Editor: Agostina Chiavola

Received: 12 October 2024
Revised: 22 November 2024
Accepted: 4 December 2024
Published: 9 December 2024

1. Introduction

Climate change disproportionately impacts coastal communities. With ever growing coastal populations [1] and the largest cities in the world being located in coastal zones, there is a pressing need to identify easily scalable strategies to protect coastal zones [2]. The most effective and commonly used climate interventions are engineered built infrastructure for coastal defense [3]. While such structures have become increasingly popular around the world [4], they result in changes to the local sediment composition and dynamics, eventually impacting the local habitat and ecosystem [5]. The use of materials sourced on-site and from the ocean would avoid such unintended impacts. Calcareous deposits that form on metal structures exposed to seawater is one such promising option [6].

Calcareous deposits are a result of electrochemical reactions leading to the precipitation of a mixture of $CaCO_3$ and $Mg(OH)_2$ from seawater. These deposits have been beneficially used to support and rejuvenate coral reefs [7,8], create sustainable concrete [9,10], prevent the corrosion of metal infrastructure [11–13], and more recently as a means to capture and remove CO_2 from seawater [14–18]. Though beneficial in these cases, calcareous deposits can prove detrimental to other electrochemical processes by causing scale formation on membranes, electrodes, and flowlines [19–22]. Due to the many applications and issues posed by calcareous deposits, the process has been widely researched and reviewed [12,23,24].

Prior studies on calcareous deposits have highlighted the sensitivity of the deposit composition and properties to various process conditions and the need for dedicated research into optimizing the process for each application. For example, to use calcareous

deposits for coastal defense infrastructure, the mechanical strength of the precipitate is critical, which in turn is determined by the relative composition of $CaCO_3$ and $Mg(OH)_2$ in the precipitate. The $Mg(OH)_2$ is flaky and breaks off or undergoes dissolution, making it less ideal for structural applications [25], so $CaCO_3$-rich calcareous deposits are desirable.

In seawater, the major electrochemical reactions involved in the formation of calcareous deposits are the hydrolysis of water, the conversion of dissolved oxygen into hydroxyl ions, and the formation of chlorine gas with the generation of hydroxyl ions increasing local pH to induce the precipitation of $CaCO_3$ and $Mg(OH)_2$ as shown in Equations (1)–(5) below and in Figure 1a. Additional reactions can also occur in the system such as shifts in the bicarbonate/carbonate equilibrium and hypochlorite generation from the reaction of the generated Cl_2 and OH^-; such side reactions minimize the rapid increase in the solution's pH. Through a combination of electrochemical cell design and processing parameters, the side reactions can be accelerated or minimized, but such efforts are beyond the scope of this study. Other potential precipitation reactions such as the precipitation of $MgCO_3$ and $Ca(OH)_2$ are not observed during the electrochemical deposition due to slow reaction kinetics for $MgCO_3$ and greater solubility for $Ca(OH)_2$, requiring more extreme changes in solution pH before precipitating [26,27].

$$O_{2(g)} + 2H_2O + 4e^- \rightarrow 4OH^-_{(aq)} \quad (1)$$

$$2H_2O + 2e^- \rightarrow H_{2(g)} + 2OH^-_{(aq)} \quad (2)$$

$$2Cl^-_{(aq)} \rightarrow Cl_{2(g)} + 2e^- \quad (3)$$

$$2OH^-_{(aq)} + Mg^{2+}_{(aq)} \leftrightarrow Mg(OH)_{2(s)} \quad (4)$$

$$OH^-_{(aq)} + HCO^-_{3(aq)} + Ca^{2+}_{(aq)} \leftrightarrow CaCO_{3(s)} + H_2O \quad (5)$$

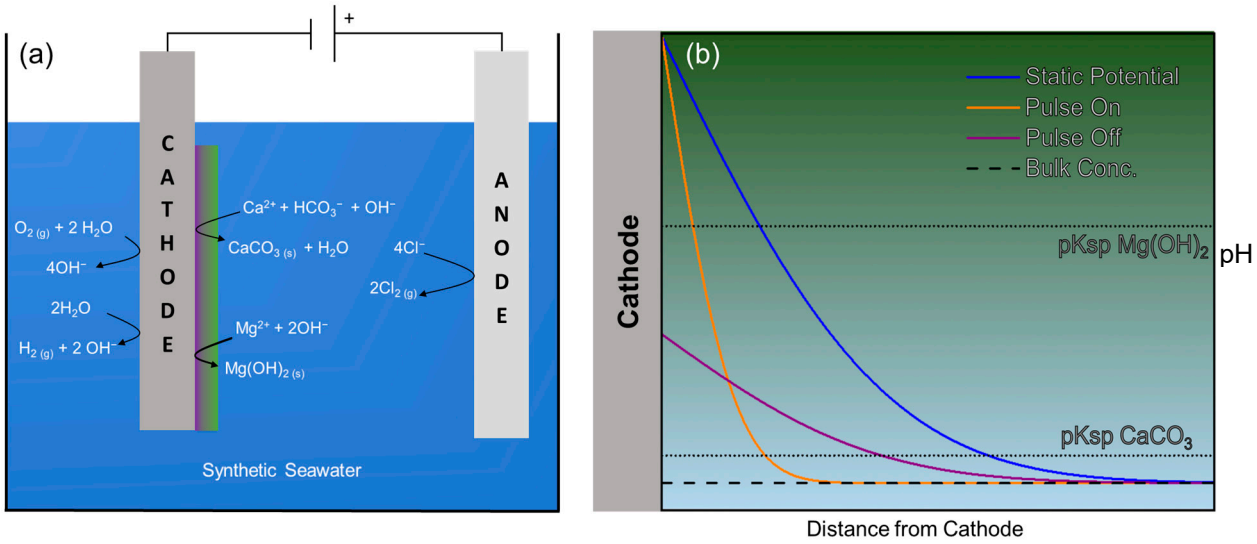

Figure 1. (**a**) Schematic showing the key electrochemical and precipitation reactions occurring at the anode and cathode during calcareous electrodeposition. The precipitation reaction products of $CaCO_3$ and $Mg(OH)_2$ are shown in green and purple, respectively. (**b**) Approximate trends in pH at different distances from the electrode under different applied potential profiles obtained using a planar source model. pKsp lines for $Mg(OH)_2$ and $CaCO_3$ are included to help visualize where $Mg(OH)_2$ and $CaCO_3$ precipitation reactions are dominant.

The precipitation reactions for $Mg(OH)_2$ and $CaCO_3$ occur at different pH values with reported pKsp values of 10.9 and 8.4, respectively, in seawater at 25 °C [23]. For $Mg(OH)_2$ specifically, the critical pH value to observe any precipitate was found to be 9.3 when testing in a seawater matrix free of $CaCl_2$ [28]. This difference in precipitation pH allows

for different compositions of deposit to form based on the voltage or current applied to the system. When applying constant voltage, the chemical reactions near the electrodes can be controlled by selecting a voltage below the activation potential of undesired side reactions but sufficient for the activation of target reactions. In seawater, the main two reactions that need to be controlled are the oxygen reduction and hydrolysis reaction noted in Equations (1) and (2). The reduction of oxygen in water is known to have an activation potential around −0.45 V vs. SCE while the hydrolysis reaction has an activation potential around −1.05 V vs. SCE [29]. Maintaining a cathode potential below the activation of the hydrolysis reaction will prevent it from occurring while only moderately increasing local pH around the cathode through O_2 reduction. With the need for oxygen to diffuse to the cathode for this reaction to take place, the pH only slightly increases around the cathode as the reaction rate is limited, which favors the formation of $CaCO_3$. When applying a voltage that exceeds the activation potential for the hydrolysis reaction, no diffusion is necessary for the reaction, and the pH increases rapidly, allowing for $Mg(OH)_2$ to precipitate in large quantities along with evolution of hydrogen gas as noted in Equation (2). With bubbles forming at the same time as precipitation, the deposit generated will be porous and have cracks, which is not ideal for corrosion protection. In addition to differences in applied voltage and current profiles, differences in cation and anion concentration, temperature, electrode, and presence of organic molecules have all been shown to impact the composition and characteristics of the resulting deposits [24,28–36].

Though calcareous deposits have been well studied, investigation into how applying a pulsed-voltage profile influences the composition of the precipitates has received minimal attention. One of the potential benefits of using a pulsed voltage is the ability to have greater control over the composition and thickness of the film formed on to the electrode [37]. Given that the reaction to form $CaCO_3$ and $Mg(OH)_2$ is pH dependent, being able to control the local concentration of OH^- near the electrode using the pulsed field would allow control over the deposit composition. We illustrate the differences in local pH near the electrode under the static and pulsed potential scenarios as a function of distance from the cathode in Figure 1b. Under a pulsed potential, the generated OH^- ions from the pulse-induced electrochemical reactions are allowed to diffuse away from the cathode surface when the pulse is turned off, ensuring that the local pH increase is limited and does not exceed the critical pH for $Mg(OH)_2$ precipitation as shown by the pKsp threshold. In addition to controlling the local pH at the cathode, the pulse-off phase also allows for the diffusion of reactants to the cathode surface, permitting increased reaction rates during the subsequent pulse-on phase. Therefore, by manipulating the voltage pulses, the local pH can be controlled to result in electrodeposits rich in $CaCO_3$.

Some of the earliest investigations into the pulse electrodeposition of calcareous deposits were conducted by Zamanzade et al. [38–40]. In their experiments, they used a rotating disc electrode configuration and examined the influence of factors such as temperature, electrode rotation speed, Ca^{2+} and Mg^{2+} concentration, and the frequency of the pulses. Their work showed that by changing the frequency of the pulses, the resulting deposit composition would also be altered. It was shown that $Mg(OH)_2$ is favored at low frequency, while $CaCO_3$ in the form of aragonite is favored at high frequency [39]. More recently, Tu and Cottis have reported an optimum frequency for aragonite formation to be 100 Hz when applying a 50% duty cycle between current densities of 1 and 0 mA/cm^2 in the context of corrosion prevention [41]. While these studies demonstrate the feasibility of using pulse electrodeposition to control composition and obtain $CaCO_3$-rich materials, an accurate evaluation of Ca/Mg ratios in the deposits as a function of pulsing conditions is not reported but is critical to determining the feasibility of the approach for several applications.

In this study, a pulsed applied potential with varying frequencies and duty cycles is applied to a low-carbon steel cathode and inert anode to form a calcareous deposit and subsequently analyzed by inductively coupled plasma mass spectrometry (ICP-MS) to determine the concentration ratio of Ca/Mg in the deposit. This is the first investigation that uses analytical methods to track the composition of the deposit under different applied

potential conditions to inform pulse-control strategies to maximize $CaCO_3$ content, which is desired for diverse applications.

2. Materials and Methods

Electrodeposition experiments were conducted using a 3-electrode cell with a 1 cm × 6 cm × 0.0635 cm low-carbon steel cathode (made from shim stock acquired from McMaster Carr), a Ag/AgCl reference electrode (leakless mini from eDAQ), and a Pt anode (Pt-coated Ti mini-electrode from eDAQ). To minimize the variability in electrode spacing from one experiment to the next, a custom-designed Teflon plate electrode holder was used (see Figure S1). The synthetic seawater electrolyte was prepared using Instant Ocean® salt mix according to the package instructions (36 g of salt dissolved in 1 L of DI water). All experiments were conducted in duplicate under ambient conditions and lasted a minimum of 72 h to generate sufficient deposits for characterization in a solution volume large enough to experience only minimal changes in pH and concentrations over the course of the experiment. The voltage input anddata collection during the electrodeposition experiments was conducted using a VSP-300 potentiostat (BioLogic, Seyssinet-Pariset, France) and associated EC-lab software (V11.42). This study investigated constant voltage at −0.8 V and −1.2 V vs. SCE, based on the onset potentials for competing electrochemical side reactions (i.e., steel corrosion reaction >−0.65 V vs. SCE, O_2 reduction reaction <−0.45 V vs. SCE, and H_2O reduction reaction <−1.05 V vs. SCE). The pulsed-voltage experiments used the same voltage bounds (−0.8 V and −1.2 V vs. SCE) and pulse frequencies of 1, 10, and 100 Hz. The viable pulse frequency was determined through initial experiments that spanned a larger frequency range and did not show rapid degradation of the cathode (see Figure S2). The fraction of time the pulse is on is defined as a duty cycle, and experiments used 10, 30, and 50% duty cycles at a 10 Hz pulse frequency to investigate the influence of duty cycle on deposit composition.

All electrodes were carefully weighed before and after the experiment to obtain the deposit mass. The electrodes were dried in an oven overnight before taking post-experimental mass to account for any residual water. Mass losses due to cathode dissolution during the experiment were small due to the protective nature of the electrodeposit. To prepare the deposits for compositional analysis, the samples were washed with DI water to remove any salts that may have crystallized on the electrode surface upon electrolyte evaporation. The washed deposits were characterized by X-ray diffraction (XRD) using a powder X-ray diffractometer (Bruker D8 Discover Microfocus, Billerica, MA, USA) equipped with a Cu source. Scans were conducted using an accelerating voltage of 50 kV and current of 1000 mA and between 10 and 90° (2θ) at a step size of 0.02°. Simulated XRD patterns were generated using Mercury software (ver. 2024.2.0 (Build 415171), Cambridge Crystallography Data Centre) using relevant crystal structures obtained either from the Crystallographic Open Database or original sources [42,43]. To characterize sample morphology, scanning electron microscopy (SEM) imaging was used. Images were taken at 2 kV using an Apreo variable pressure SEM (Thermo Fisher Scientific, Waltham, USA). Energy dispersive X-ray spectroscopy (EDS) analysis was performed using a Phillips XL30 system to investigate the distribution of Ca/Mg in the sample.

To accurately measure the Ca and Mg composition of the deposits, ICP-MS analysis was performed using a Perkin Elmer NexION 2000 (Hopkinton, MA, USA) instrument. Samples were prepared by weighing deposits in a microanalytical balance and digesting in acid (70% by volume HNO_3) for a concentration of 5 g/L. The acid digestion was performed for over 48 h, and the resulting solutions were subjected to serial dilution so that the concentration of solutes was <200 µg/L and within the desired range for ICP-MS analysis. An internal scandium reference was used to calibrate the readings. The raw data were processed to obtain the Ca/Mg composition of the deposits.

3. Results and Discussion

To establish the impact of using a pulse voltage profile, baseline experiments were conducted at constant voltage, specifically at −0.8 V vs. SCE and −1.2 V vs. SCE, which were the limits of the voltage window used for the pulsed electrodeposition. The deposits formed on the low-carbon steel electrode (Figure 2a) were first examined by XRD (Figure 2b) to see how the different parameters of voltage and frequency impacted the crystallinity of the deposits. There were no observable changes in the XRD patterns of samples obtained from pulsed voltage compared with those from constant −0.8 V vs. SCE experiments. All samples were identified to contain majority aragonite-$CaCO_3$ (Figure 2b). Under a constant applied voltage of −1.2 V vs. SCE, the samples were primarily brucite, a polymorph of $Mg(OH)_2$, and the broad XRD peaks suggested poor sample crystallinity, in agreement with past reports on brucite electrodeposits [28,29,41]. Investigation of the morphology of constant-voltage electrodeposits using SEM showed mostly needle-like structures in aragonite-rich samples (Figure 2c) and platelet-like structures in brucite-rich samples (Figure 2d). The pulsed electrodeposits were aragonite-rich with needle-like morphology (see Figures S3–S5) similar to the deposit generated at −0.8 V vs. SCE. In addition to these crystal forms, there were dendrite and ribbon structures on the deposit as shown in Figure 2e. Based on further SEM and EDS analyses (Figures S6 and S7), the amorphous regions were identified as being primarily composed of Na in the case of dendritic structures and composed of Mg in the case of ribbon-like structures. The Na-rich regions were also Cl-rich, suggesting they were NaCl salt deposits that were produced upon electrolyte drying on the electrode surface. Such Na-rich deposits in SEM images were observed to be covering needle-like aragonite (Figure S7), confirming that they were surface deposits on top of the electrolytically grown structures. Similarly, there were other major elements of seawater observed in the samples (Figure S8). The presence of these salts is not correlated with electrodeposition conditions but rather the sample extraction and drying process.

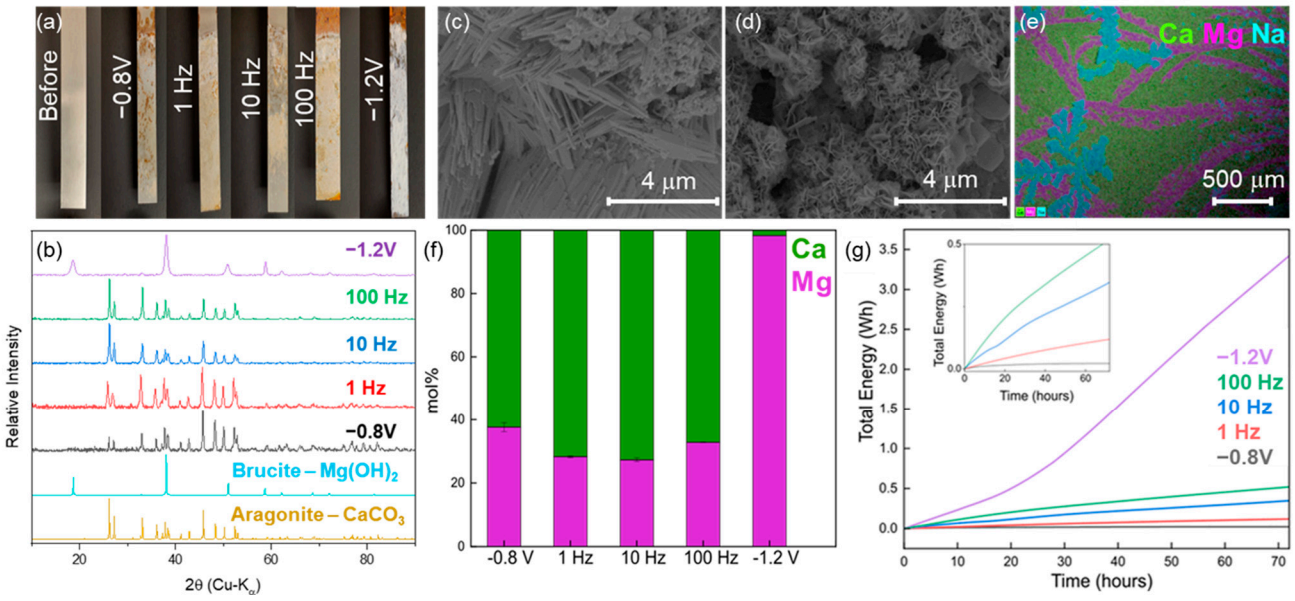

Figure 2. (**a**) Steel cathodes with electrodeposits before and after each applied potential condition. (**b**) Powder XRD patterns for deposits obtained for constant and pulsed potential experiments under a 10% duty cycle along with reference patterns for Aragonite-$CaCO_3$ and Brucite-$Mg(OH)_2$. Representative SEM images of (**c**) aragonite-rich deposits from −0.8 V vs. SCE experiment and (**d**) brucite-rich sample from −1.2 V vs. SCE experiment. (**e**) EDS images of 1 Hz pulse potential deposits showing Mg, Ca, and Na distributions across the sample. (**f**) Measured mol% of Ca and Mg in electrodeposits obtained under different potential profiles using ICP-MS. (**g**) Measured energy use for each experimental condition. Inset graph is a zoom-in of the data set between 0 and 0.5 Wh.

Under pulsed electrodeposition vs. constant voltage experiments, we expect oscillations in pH near the electrode, resulting in different distributions and ratios of $CaCO_3$ and $Mg(OH)_2$ precipitation as the deposit grows farther away from the electrode surface. To investigate the spatial variability in Mg vs. Ca in the electrodeposits, we used EDS (Figures 2e, S9 and S10). Our images clearly highlight the presence of distinct domains that are rich in Mg and Ca. Furthermore, while the Mg-rich regions do not show measurable Ca, the Ca-rich regions always contain low levels of Mg. This observation is consistent with the established understanding that $CaCO_3$ does not deposit on steel without a layer of brucite deposit on the electrode first [31,33,34]. This result suggests that completely eliminating $Mg(OH)_2$ from the deposit is not possible without further modification of the electrode surface to promote direct $CaCO_3$ deposition. Under pulsed conditions, the higher frequency pulses may allow a thin $Mg(OH)_2$ layer to deposit faster and more thinly before being covered by an initial layer of $CaCO_3$ in the pulse-off phase, allowing for Ca-rich deposits in the subsequent pulse-on phase.

To understand the rates of electrodeposition under the different conditions, the mass of the deposits was recorded for each experiment (Table 1). The data show an increase in deposit mass as a function of frequency when compared to a constant voltage of −0.8 V vs. SCE. The highest deposit mass was obtained under a constant voltage of −1.2 V vs. SCE, which was ~8× more than that obtained at −0.8 V vs. SCE. The observed trend in deposit mass is correlated with the highest applied voltage for each experiment. The higher voltages allow for water electrolysis reactions to occur, generating higher pH and leading to more precipitate deposition. However, most of the deposits obtained at −1.2 V vs. SCE are $Mg(OH)_2$, as the local pH escalates well above the pKsp for $Mg(OH)_2$ allowing for Mg-rich deposits to rapidly form on the electrode. By pulsing the voltage, this pH escalation is avoided, resulting in $CaCO_3$-rich electrodeposits. However, under pulsed conditions, a lower deposit mass is obtained. When the duty cycle for a given frequency of pulsing is increased, it results in applying higher voltages for longer periods of time, thereby increasing both the Mg content and the total mass of the deposits. By increasing the duty cycle from 10% to 30% and 50% for the 10 Hz condition, the deposited mass was observed to increase, with a significant increase in mass for 50% duty cycle, indicating that the pH may not be as well controlled, leading to significant $Mg(OH)_2$ precipitation.

Table 1. Deposit mass after 72 h under constant and pulse potential profiles, with varying pulse frequency and duty cycle (DC).

Experiment	Trial 1 Mass (mg)	Trial 2 Mass (mg)	Mass Average (mg)	Energy per g $CaCO_3$ (Wh/g)
Constant −0.8 V	17.2	21.7	19.5	1.53
1 Hz DC 10	18.9	24.2	21.6	6.77
10 Hz DC 10	21.3	16.9	19.1	22.2
100 Hz DC 10	24.4	22.6	23.5	28.4
Constant −1.2 V	160.9	190.3	175.6	676
10 Hz DC 30	23.5	27.0	25.3	53.1
10 Hz DC 50	69.4	49.6	59.5	55.2

To quantify the Ca/Mg ratio in the deposits, ICP-MS analysis was conducted, the results of which are shown in Figure 2f. The data show that the pulsed experiments increased the fraction of Ca-rich deposits over the baseline experiment conducted at −0.8 V vs. SCE. The Ca/Mg molar ratio reached a maximum for the 10 Hz experiments, with a molar ratio of 2.7, which is roughly 73 mol% Ca and 27 mol% Mg. The relatively high amounts of Mg measured by ICP-MS and the absence of brucite peaks in the XRD analysis of the pulse electrodeposition samples suggest the Mg compounds to be amorphous in nature. Further enhancing the frequency of the pulsed experiments to 100 Hz did not result in additional amplification of the Ca/Mg molar ratio, indicating that there is an optimized frequency that enhances the amount of $CaCO_3$ deposited for the given test conditions. The

decrease in favorability for $CaCO_3$ deposition at higher frequency pulsing could be just a result of the system experiencing longer durations closer to −1.2 V vs. SCE from the slow kinetics of electrode polarity switching, combined with mass transport limitations that restrict the rapid diffusion of OH^- ions away from the electrode surface, allowing the local pH to linger above the critical pH value of 9.3 to induce more $Mg(OH)_2$ precipitation over $CaCO_3$. The experiment conducted at a constant voltage of −1.2 V vs. SCE almost exclusively deposited Mg (98.3 mol%) on the electrode. We note that in general the EDS results suggested higher Ca/Mg ratios than ICP-MS as the technique is surface-sensitive and does not fully factor in the $Mg(OH)_2$ layer on the electrode that is underneath the aragonite-$CaCO_3$.

Though the $CaCO_3$ content is shown to increase when a low duty cycle is used, the energy expenditure for the applied pulses adds significantly to the energy cost of carbonate mineralization. As shown in Figure 2g, the energy expenditure for applying a constant −0.8 V is significantly lower (0.022 Wh) than all the pulsed profiles considered here. The next lowest measured energy consumption value was 0.119 Wh from the 1 Hz 10% duty cycle case, showing a 5× increase in energy consumption with a 4.4× increase in energy used per gram of $CaCO_3$ generated (Table 1). The low energy consumption in the constant −0.8 V vs. SCE case is likely due to deposit layer becoming thick and electrically insulating, limiting the occurrence of key electrolysis reactions (Equations (1) and (2)). This causes the electrode to experience a low current and effectively reaches a saturation point where no more deposit is being formed without the expenditure of any energy. For the pulsed samples, the marginal gains in deposit mass when compared to the added energy expenditure suggests that the pulse-on phase drives forward the electrolysis reactions but does not generate a local pH high enough to induce larger gains in deposit mass. The energy consumption for the −1.2 V vs. SCE sample and larger mass suggests that the deposit formation at this voltage is not as limited, when it comes to generating a sufficient local pH to drive precipitation. The deposit from this constant voltage case is primarily brucite, but applying a larger duty cycle in the pulsed cases could lead to more deposit mass with a stronger preference for $CaCO_3$ formation.

Based on the fact that the most Ca-rich deposits were obtained with 10 Hz pulse frequency, subsequent experiments were conducted at this frequency, with higher duty cycles (30% and 50%). ICP-MS characterization and total energy consumption of the resulting electrodeposits are shown in Figure 3a–c. From the XRD data, all samples were identified to be aragonite-$CaCO_3$ with no variability in the degree of sample crystallinity. While XRD showed no presence of $Mg(OH)_2$, ICP-MS analysis of the digested deposits highlights the presence of considerable amounts of Mg in all samples. The Mg content of the deposits increased from 27 mol% in 10% duty cycle to 54.0 mol% and 69.5 mol% in 30% and 50% duty cycle experiments, respectively. This indicates that either the Mg deposits are amorphous or poorly crystallized. The SEM image of the 10 Hz duty cycle 50% (Figure S11) shows a significant amount of amorphous material in between aragonite pillars, further supporting that the Mg deposits may not be detected by XRD. Though the total deposit mass increased as expected, the selectivity for $CaCO_3$ is lost when higher duty cycles are used. It may be possible to slowly ramp up the duty cycle to increase the deposit mass without compromising the selectivity for $CaCO_3$, but the overall energy usage, as shown in Figure 3c, increases with duty cycle, making it a less attractive approach for processes trying to minimize their energy or CO_2 footprint. Thicker and denser deposits with $CaCO_3$ can be worth it in the context of corrosion prevention as a thicker layer can help prevent the corrosion of underlying metal structures, especially for structures deployed within seawater.

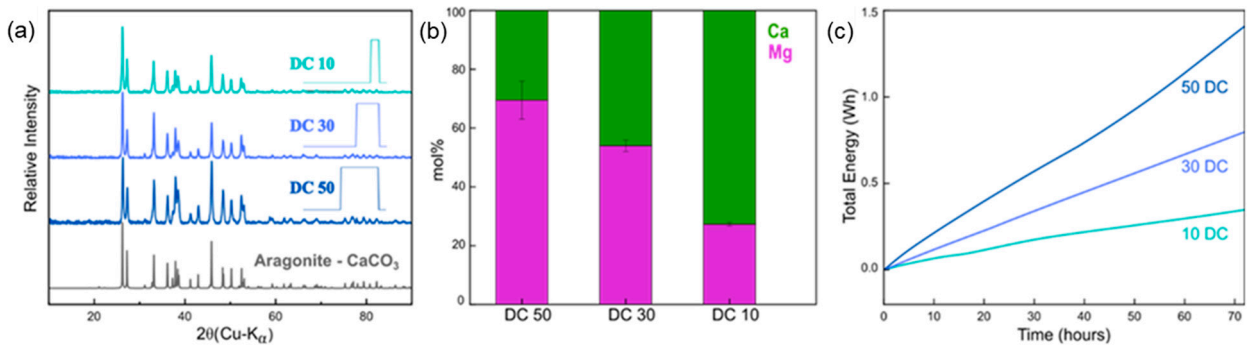

Figure 3. (**a**) XRD patterns for deposits obtained under 10 Hz pulse frequency and variable DC compared to a reference Aragonite pattern. The inset is a visual representation of the 10, 30, and 50% DC pulse profiles. (**b**) Measured mol% of Ca and Mg in samples from 10 Hz pulse frequency with variable DC using ICP-MS. (**c**) Measured energy consumption of the 10 Hz samples at different duty cycles.

Our results show that pulsed voltage with shorter duty cycles offers control over the interfacial pH to maximize precipitation of $CaCO_3$. Given that the $CaCO_3$ deposits are denser and less prone to dissolution/reprecipitation than $Mg(OH)_2$, the pulse voltage electrodeposits have more desirable mechanical properties for coastal construction and anti-corrosion applications. Further, pulse voltage could also be used for the reduction in $Mg(OH)_2$ deposition on electrodes used in ocean-based electrochemical processes to suppress scaling-related inefficiencies. For example, Kim et al. recently demonstrated an electrochemical marine CO_2 removal technique using Ag/AgCl and Bi/BiOCl electrodes [22], where a key factor limiting process performance was the formation of $Mg(OH)_2$ precipitates on the electrodes. Voltage pulsing in such systems could reduce some of the observed precipitation.

4. Conclusions

In this work, the impact of using a pulsed voltage on the composition of calcareous electrodeposits was investigated. Generally, $CaCO_3$ and $Mg(OH)_2$ are co-precipitated, and maximizing the $CaCO_3$ content in the deposits offers enhanced mechanical strength, which is relevant for coastal structures and for carbon mineralization applications. The reduced $Mg(OH)_2$ precipitation could also be of value to minimizing scale formation on electrodes in marine electrochemical systems. Pulsed voltage controls the interfacial pH at the electrode which dictates the precipitation reactions. We conducted experiments under constant and pulsed-voltage conditions, with pulsed experiments varying the pulsing frequencies and duty cycles. The electrodeposits were characterized for their composition, morphology, and Ca/Mg content to determine experimental conditions that would result in $CaCO_3$-rich deposits. Lower duty cycles and frequencies resulted in more Ca-rich precipitates, while higher frequencies resulted in more deposit mass. Our data show factors such as voltage boundaries, pulse frequency, and duty cycles to impact the deposit composition and deposition rates. We demonstrate the utility of pulse electrodeposition for the formation of calcareous deposits, but dedicated optimization will be needed to achieve the target deposit composition for a given application and to obtain faster deposition rates for the process to be relevant for practical use. Further, cost–benefit analyses of using pulse electrodeposition will need to factor project siting, sources of electricity, etc., when it comes to determining its efficacy for sustainability-focused end uses.

Supplementary Materials: The following supporting information can be downloaded at: https://www.mdpi.com/article/10.3390/su162310776/s1, Figure S1: Experimental set-up used in this study. Figure S2: Preliminary experiments used to identify suitable electrochemical parameters. Figures S3–S7: SEM images of deposits obtained under different voltage conditions. Figures S8–S10: EDX data for the 1Hz sample shown in Figure 2e,f of the main manuscript. Figures S11 and S13:

Representative SEM image of deposit from 10Hz pulsing at 50% and 30% duty cycle. Figure S12: XRD of unwashed deposits showing presence of NaCl. Figure S14: Electrode photographs after long-term storage in air.

Author Contributions: A.J.R. conducted the experiments and performed the data analysis, with characterization support from Q.W. and E.A.R., while D.G. and C.V.S. were responsible for project conceptualization, management, and funding acquisition. All authors have read and agreed to the published version of the manuscript.

Funding: This research was funded by the U.S. Department of Energy (DOE) Water Power Technologies Office. Work was conducted by the Pacific Northwest National Laboratory (PNNL) in collaboration with the National Renewable Energy Laboratory (NREL). PNNL is operated by Battelle for DOE under Contract DEAC05-76RL01830, and NREL is operated by Alliance for Sustainable Energy, LLC, for DOE under Contract No. DE-AC36-08GO28308. The views expressed in this article do not necessarily represent the views of the DOE or the U.S. Government.

Institutional Review Board Statement: Not applicable.

Informed Consent Statement: Not applicable.

Data Availability Statement: Additional results and analysis can be found in the Supplementary Information (SI) document associated with this article. All experimental data included in the main manuscript and SI, are available from the corresponding author upon request.

Acknowledgments: We acknowledge use of equipment acquired with support from the PNNL Laboratory Directed Research and Development Program (LDRD) for this study. Part of this work was conducted at the Molecular Analysis Facility, a National Nanotechnology Coordinated Infrastructure (NNCI) site at the University of Washington with partial support from the National Science Foundation via awards NNCI-2025489 and NNCI-1542101. We thank Eric Spear for initial work and Lola González Olías for valuable discussions.

Conflicts of Interest: The authors declare no competing financial interests.

References

1. Crossett, K.; Ache, B.; Pacheco, P.; Haber, K. National coastal population report, population trends from 1970 to 2020. In *NOAA State of the Coast Report Series*; US Department of Commerce: Washington, DC, USA, 2013.
2. Sandifer, P.A.; Scott, G.I. Coastlines, Coastal Cities, and Climate Change: A Perspective on Urgent Research Needs in the United States. *Front. Mar. Sci.* **2021**, *8*, 631986. [CrossRef]
3. Bulleri, F.; Chapman, M.G. The introduction of coastal infrastructure as a driver of change in marine environments. *J. Appl. Ecol.* **2010**, *47*, 26–35. [CrossRef]
4. Hanak, E.; Moreno, G. California coastal management with a changing climate. *Clim. Change* **2012**, *111*, 45–73. [CrossRef]
5. Firth, L.B.; Mieszkowska, N.; Thompson, R.C.; Hawkins, S.J. Climate change and adaptational impacts in coastal systems: The case of sea defences. *Environ. Sci. Process. Impacts* **2013**, *15*, 1665. [CrossRef]
6. Li, C.J.; Du, M. The growth mechanism of calcareous deposits under various hydrostatic pressures during the cathodic protection of carbon steel in seawater. *RSC Adv.* **2017**, *7*, 28819–28825. [CrossRef]
7. Goreau, T.J.F. Coral Reef Electrotherapy: Field Observations. *Front. Mar. Sci.* **2022**, *9*, 805113. [CrossRef]
8. Hilbertz, W.H. Electrodeposition of minerals in sea water: Experiments and applications. *IEEE J. Ocean. Eng.* **1979**, *4*, 94–113. [CrossRef]
9. Johra, H.; Margheritini, L.; Ivanov Antonov, Y.; Meyer Frandsen, K.; Enggrob Simonsen, M.; Møldrup, P.; Lund Jensen, R. Thermal, moisture and mechanical properties of Seacrete: A sustainable sea-grown building material. *Constr. Build. Mater.* **2021**, *266*, 121025. [CrossRef]
10. Li, B.; Jiang, Z.; Zhou, G.; Chen, Q. The effect of Ca^{2+} concentrations on the characteristics of $Mg(OH)^{2-}$ based building materials prepared in situ by electrodeposition. *Constr. Build. Mater.* **2021**, *271*, 121523. [CrossRef]
11. Metwally, I.A.; Al-Badi, A.H. Analysis of different factors affecting cathodic protection for deep well casings. *Mater. Corros.* **2010**, *61*, 245–251. [CrossRef]
12. Hartt, W.H.; Culberson, C.H.; Smith, S.W. Calcareous Deposits on Metal Surfaces in Seawater—A Critical Review. *Corrosion* **1984**, *40*, 609–618. [CrossRef]
13. Sun, W.; Liu, G.; Wang, L.; Li, Y. A mathematical model for modeling the formation of calcareous deposits on cathodically protected steel in seawater. *Electrochim. Acta* **2012**, *78*, 597–608. [CrossRef]
14. Alturki, A. The Global Carbon Footprint and How New Carbon Mineralization Technologies Can Be Used to Reduce CO_2 Emissions. *ChemEngineering* **2022**, *6*, 44. [CrossRef]

15. Bustillos, S.; Prentice, D.; La Plante, E.C.; Wang, B.; Sant, G.; Simonetti, D. Process Simulations Reveal the Carbon Dioxide Removal Potential of a Process That Mineralizes Industrial Waste Streams via an Ion Exchange-Based Regenerable pH Swing. *ACS Sustain. Chem. Eng.* **2022**, *10*, 6255–6264. [CrossRef]
16. La Plante, E.C.; Chen, X.; Bustillos, S.; Bouissonnie, A.; Traynor, T.; Jassby, D.; Corsini, L.; Simonetti, D.A.; Sant, G.N. Electrolytic Seawater Mineralization and the Mass Balances That Demonstrate Carbon Dioxide Removal. *ACS EST Eng.* **2023**, *3*, 955–968. [CrossRef]
17. Vibbert, H.B.; Park, A.-H.A. Harvesting, storing, and converting carbon from the ocean to create a new carbon economy: Challenges and opportunities. *Front. Energy Res.* **2022**, *10*, 999307. [CrossRef]
18. Zhao, Y.; Wang, J.; Ji, Z.; Liu, J.; Guo, X.; Yuan, J. A novel technology of carbon dioxide adsorption and mineralization via seawater decalcification by bipolar membrane electrodialysis system with a crystallizer. *Chem. Eng. J.* **2020**, *381*, 122542. [CrossRef]
19. Digdaya, I.A.; Sullivan, I.; Lin, M.; Han, L.; Cheng, W.-H.; Atwater, H.A.; Xiang, C. A direct coupled electrochemical system for capture and conversion of CO_2 from oceanwater. *Nat. Commun.* **2020**, *11*, 4412. [CrossRef]
20. Edvardsen, L.; Gawel, K.; Wenner, S.; Gawel, B.; Torsæter, M. Electrochemical enhancement and inhibition of calcium carbonate deposition. *J. Environ. Chem. Eng.* **2020**, *8*, 104239. [CrossRef]
21. Liu, Y.; Lucas, É.; Sullivan, I.; Li, X.; Xiang, C. Challenges and opportunities in continuous flow processes for electrochemically mediated carbon capture. *iScience* **2022**, *25*, 105153. [CrossRef]
22. Kim, S.; Nitzsche, M.P.; Rufer, S.B.; Lake, J.R.; Varanasi, K.K.; Hatton, T.A. Asymmetric chloride-mediated electrochemical process for CO_2 removal from oceanwater. *Energy Environ. Sci.* **2023**, *16*, 2030–2044. [CrossRef]
23. Carré, C.; Zanibellato, A.; Jeannin, M.; Sabot, R.; Gunkel-Grillon, P.; Serres, A. Electrochemical calcareous deposition in seawater. *A review. Environ. Chem. Lett.* **2020**, *18*, 1193–1208. [CrossRef]
24. Yeo, L.M.; Kurniawan, D. Parameters related to seawater conditions and electrodeposition setting on the growth of formation of calcareous deposit: A review. *AIP Conf. Proc.* **2020**, *2262*, 070001. [CrossRef]
25. Thomas, J.G. Marine Electrolysis for Building Materials and Environmental Restoration. In *Electrolysis*; Vladimir, L., Janis, K., Eds.; IntechOpen: Rijeka, Croatia, 2012; Chapter 13.
26. Santos, H.S.; Nguyen, H.; Venâncio, F.; Ramteke, D.; Zevenhoven, R.; Kinnunen, P. Mechanisms of Mg carbonates precipitation and implications for CO_2 capture and utilization/storage. *Inorg. Chem. Front.* **2023**, *10*, 2507–2546. [CrossRef]
27. Irving, L. The precipitation of calcium and magnesium from sea water. *J. Mar. Biol. Assoc. UK* **1926**, *14*, 441–446. [CrossRef]
28. Deslouis, C.; Festy, D.; Gil, O.; Maillot, V.; Touzain, S.; Tribollet, B. Characterization of calcareous deposits in artificial sea water by impedances techniques: 2-deposit of $Mg(OH)_2$ without $CaCO_3$. *Electrochim. Acta* **2000**, *45*, 1837–1845. [CrossRef]
29. Barchiche, C.; Deslouis, C.; Festy, D.; Gil, O.; Refait, P.; Touzain, S.; Tribollet, B. Characterization of calcareous deposits in artificial seawater by impedance techniques: 3—Deposit of $CaCO_3$ in the presence of Mg(II). *Electrochim. Acta* **2003**, *48*, 1645–1654. [CrossRef]
30. Kitano, Y.; Hood, D.W. The influence of organic material on the polymorphic crystallization of calcium carbonate. *Geochim. Cosmochim. Acta* **1965**, *29*, 29–41. [CrossRef]
31. Krauss, C.; Chateigner, D.; Gil, O. Fully Inorganic Electrodeposition of Pure Aragonite Prismatic-like Textured Layers on Titanium Foils. *Cryst. Growth Des.* **2008**, *8*, 4378–4382. [CrossRef]
32. Mucci, A.; Canuel, R.; Zhong, S. The solubility of calcite and aragonite in sulfate-free seawater and the seeded growth kinetics and composition of the precipitates at 25 °C. *Chem. Geol.* **1989**, *74*, 309–320. [CrossRef]
33. Neville, A.; Morizot, A.P. Calcareous scales formed by cathodic protection—An assessment of characteristics and kinetics. *J. Cryst. Growth* **2002**, *243*, 490–502. [CrossRef]
34. Barchiche, C.; Deslouis, C.; Gil, O.; Refait, P.; Tribollet, B. Characterisation of calcareous deposits by electrochemical methods: Role of sulphates, calcium concentration and temperature. *Electrochim. Acta* **2004**, *49*, 2833–2839. [CrossRef]
35. Berner, R.A. The role of magnesium in the crystal growth of calcite and aragonite from sea water. *Geochim. Cosmochim. Acta* **1975**, *39*, 489–504. [CrossRef]
36. Chen, Z.; Wang, X.; Li, Z.; Ying, H.; Yang, W. Influence of Different Ions on Pulse Electrodeposition of $CaCO_3$ Scales in the Simulated Seawater. *Langmuir* **2024**, *40*, 14641–14651. [CrossRef]
37. Chandrasekar, M.S.; Pushpavanam, M. Pulse and pulse reverse plating—Conceptual, advantages and applications. *Electrochim. Acta* **2008**, *53*, 3313–3322. [CrossRef]
38. Zamanzade, M.; Shahrabi, T.; Yazdian, A. Improvement of corrosion protection properties of calcareous deposits on carbon steel by pulse cathodic protection in artificial sea water. *Anti-Corros. Methods Mater.* **2007**, *54*, 74–81. [CrossRef]
39. Zamanzade, M.; Shahrabi, T.; Gharacheh, E.A. Application of Taguchi method for the characterization of calcareous deposits formed by pulse cathodic protection. *Mater. Corros.* **2007**, *58*, 710–715. [CrossRef]
40. Zamanzade, M.; Shahrabi, T.; Ahmadi-Gharacheh, E.; Aliofkhazraei, M. Neural networks prediction of different frequencies' effects on calcareous deposits formation under pulse cathodic protection. *Russ. J. Electrochem.* **2008**, *44*, 1113–1119. [CrossRef]
41. Tu, K.; Cottis, R.A. Controlling The Components Of Calcareous Deposit To Protect Steel Structures From Alwc With Dc And Pulse Current. Presented at the CORROSION 2009, Atlanta, Georgia, 22–26 March 2009.

42. Negro, A.D.; Ungaretti, L. Refinement of the Crystal Structure Of Aragonite. *Am. Mineral.* **1971**, *56*, 768–772.
43. Desgranges, L.; Calvarin, G.; Chevrier, G. Interlayer interactions in $M(OH)_2$: A neutron diffraction study of $Mg(OH)_2$. *Acta Crystallogr. Sect. B* **1996**, *52*, 82–86. [CrossRef]